Unlocking Non-Kasha Room Temperature Phosphorescence in Azulene-based Cocrystal

Fathima Thasnim Pattanmarthodiyil and Mahesh Hariharan*

School of Chemistry, Indian Institute of Science Education and Research Thiruvananthapuram, Vithura, Thiruvananthapuram, Kerala, India 695551

*E-mail: mahesh@iisertvm.ac.in

Supporting Information (SI)

Contents

Section A: Materials and Methods

All chemicals were obtained from commercial suppliers, and HPLC-grade solvents were employed for crystal growth. ^{1}H NMR spectra were recorded on a Bruker Avance DPX 500 MHz spectrometer using tetramethylsilane (TMS) as the internal standard. FTIR spectra were collected on a Shimadzu IR Prestige-21 FT-IR spectrometer using the KBr pellet method, with a spectral resolution of 4 cm^{-1}.

1.1 Spectroscopy Experimental Details

Kubelka-Munk absorption spectra were recorded on a PerkinElmer Lambda 950 UV-Vis-NIR spectrometer. Reflectance data of crystalline samples were measured in diffuse reflectance mode and transformed using the Kubelka-Munk function. The Kubelka-Munk model is accurate when the particle size is comparable or smaller than the excitation wavelength.[1] In crystalline samples, diffuse reflectance spectra represent combined contributions from reflection, refraction, and diffraction, without separating these effects. As a result, diffuse reflectance spectra are generally less sensitive than conventional UV-Vis absorption spectra and often appear broader compared to typical absorbance or fluorescence excitation spectra. For sample preparation, $BaSO_4$ powder was used as a diluent, with crystalline samples mixed at a 5% sample to reference weight ratio. The mixtures were then pressed into the sample holder of the integrating sphere accessory of the Shimadzu UV-3600 UV–Vis-NIR spectrophotometer, and the diffuse reflectance spectra were recorded.

Photoluminescence Measurements:

Emission measurements were performed using a Horiba Jobin Yvon Fluorolog spectrometer. Photoluminescence measurements of crystals were performed by carefully preparing the sample with an optimized number of sub-millimeter sized crystals and positioning it in a designated orientation to minimize self-absorption.[2] Gated emission and phosphorescence measurements were conducted on the same instrument equipped with a flash lamp having a pulse width of 3 µs. For these measurements, the crystal was sandwiched between two quartz pieces. The crystal samples were mounted between two quartz plates for the measurements.

1.2 X-ray Crystallography

A single crystal was mounted on a glass fibre using Infineum V8512 oil. Data were collected on a Bruker APEXII CCD area detector with graphite-monochromated Mo Kα radiation and processed using the Bruker APEX2 software package. The crystal structure was solved by direct methods and refined using Fourier techniques. Non-hydrogen atoms were refined anisotropically, while hydrogen atoms were placed in calculated positions and constrained to ride on their parent atoms using the appropriate HFIX commands in SHELX-97.[3] In the structures of Az-TCNB and Az-DITFB, Az exhibited the well-known two-component disorder around an inversion centre, which was modelled with half occupancy. All programs employed during the crystal structure analysis are integrated within the WINGX software.[4,5] Full validation of the CIF and structure factors was performed using the checkCIF utility, which confirmed the absence of any major alert levels. Three-dimensional structure visualization and examination of the crystal packing were carried out using Mercury 3.10.1.[6,7]

1.3 Computational Analysis

All calculations were performed using Gaussian 16.[8] The frontier molecular orbitals (FMOs) of cocrystals were obtained from the cube files generated in the energy calculations. Time-dependent DFT (TDDFT) calculations were carried out using the LC-ωPBE functional for accurate prediction of charge-transfer (CT) character with the def2-SVP basis set.

1.4 Symmetry Adapted Perturbation Theory (SAPT)[9]

SAPT(0) analysis was performed to evaluate the non-covalent interaction energies of molecular dimers using the SAPT module of the Psi4 program, with the aug-cc-pVDZ basis set for Az-TCNB and the def2-SVP basis set (suitable for heavy-atom containing systems) for Az-DITFB. The SAPT(0) method decomposes the total interaction energy into physically meaningful components, including first-order electrostatics and exchange, as well as second-order induction, dispersion, and their corresponding exchange terms within a second-order perturbation framework.

$$E_{int}^{SAPT(0)} = E_{elec}^{(1)} + E_{ex}^{(1)} + E_{ind}^{(2)} + E_{ind-ex}^{(2)} + E_{dis}^{(2)} + E_{dis-ex}^{(2)} \quad \text{(Equation S2)}$$

1.5 TheoDORE Analyses[10,11]

The excitations of the cocrystals were analyzed using the TheoDORE package, considering the donor and acceptor as two distinct fragments. The excited-state characteristics were evaluated using three parameters: the participation ratio (PR), the mean position (POS) of the initial orbital (hole) and final orbital (electron), and the charge transfer character (CT). The PR indicates the number of fragments involved in the excitation, with values ranging from 1 to 2 in this study. POS describes the average location of the hole and electron for a given excitation: a value of 1.5 corresponds to delocalized Frenkel states or charge-transfer states, whereas localization on monomer A or B in a dimer (AB) gives POS = 1 or POS = 2, respectively. The CT value quantifies the extent of charge separation, with CT = 1 representing a fully charge-separated state and CT = 0 corresponding to a localized Frenkel state.

1.6 Electrostatic Potential Map[12]

Electrostatic potential (ESP) maps provide a three-dimensional depiction of molecular charge distributions, enabling visualization of variably charged regions. These charge distributions inform the nature of intermolecular interactions. Gaussian[8] enables the generation of cube files directly from formatted checkpoint files through the cube keyword, using the cubegen utility, based on energy calculations performed at the LC-ωPBE/def2-SVP level of theory. This facilitates the generation of electrostatic surface potential maps for the molecule.

1.7 PySOC[13]

PySOC interfaces with Gaussian[8] and DFTB+ to evaluate spin-orbit couplings using linear-response TDDFT, TDA, and TD-DFTB methodologies. The approach employs Casida-type approximate excited-state wavefunctions in conjunction with an effective-charge Breit–Pauli Hamiltonian, while atomic integrals are generated through the MolSOC code with adapted interfaces for both Slater and Gaussian-

type basis sets.

1.8 Noncovalent Interaction (NCI) Plot[14]

NCI analysis uses an index based on electron density and its derivatives to identify noncovalent interactions. In this approach, a two-dimensional plot of reduced electron density (s) versus electron density (ρ) is constructed, where the critical points correspond to the troughs observed in the plot. The reduced electron density is formulated as:

$$\boldsymbol{s} = \frac{\mathbf{1}}{\mathbf{2}(\mathbf{3}\boldsymbol{\pi}^{\mathbf{2}})^{\mathbf{1/3}}} \frac{|\boldsymbol{\nabla\rho}|}{\boldsymbol{\rho}^{\mathbf{4/3}}} \qquad \text{(Equation S1)}$$

Noncovalent interactions occur at the real-space points corresponding to these troughs. The sign of the second derivative of ρ ($\nabla^2\rho$) is analyzed to distinguish between attractive and repulsive interactions. The noncovalent interaction regions are shown in the plot as discs, with colors ranging from blue (attractive) to red (repulsive), following the VIBGYOR spectrum.

1.9 Hirshfeld Analyses[15,16]

The intermolecular interactions within the crystal structures of the cocrystals were identified through Hirshfeld surface analysis using Crystal Explorer 3.1. The Hirshfeld surface is defined as the set of points in three-dimensional space where the ratio of promolecule to procrystal electron densities is 0.5. Intermolecular contacts were explored by mapping the normalized contact distance (d_{norm}), which is determined by the closest internal (d_i) and external (d_e) distances from a surface point to the nuclei, together with the van der Waals radii (r^{vdw}). Two-dimensional fingerprint plots were generated from the Hirshfeld surface by plotting the fraction of surface points as a function of d_i and d_e, providing a visual summary of the intermolecular contacts within the crystal system.

Section B: Synthesis and Characterization

Synthesis of Az-TCNB Cocrystal

The Az-TCNB cocrystal was synthesized through mechanochemical grinding of azulene (Az) and 1,2,4,5-Tetracyanobenzene (TCNB). The two components were combined in a 1:1 molar ratio and was ground thoroughly using a mortar and pestle. During grinding, dark blue color of donor azulene and white color of the acceptor TCNB visibly changed to brownish red, indicating the formation of the CT complex. After grinding, the resulting complex was transferred to a clean vial. To grow cocrystals, a saturated solution of the mixture was prepared in acetone (ACE) and filtered into a separate vial. The vial was left undisturbed to allow slow evaporation and the formation of cocrystal.

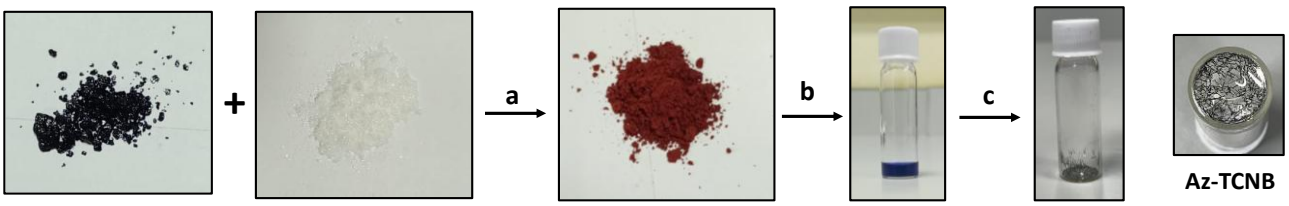

Scheme S1: (a) Mix Az and TCNB with a few drops of methanol, and grind the mixture using a mortar and pestle. Dry the resulting solid. (b) Dissolve the dried solid in acetone and filter the solution into a vial. (c) Allow the solvent to evaporate slowly over 3-4 days.

Synthesis of Az-DITFB Cocrystal[17]

The cocrystal Az-DITFB was synthesized via solvent assisted mechanochemical grinding of Az and 1,4-diiodotetrafluorobenzene (DITFB). The two components were mixed in a 1:2 molar ratio. Add few drops of methanol to the mixture and thoroughly ground using a mortar and pestle. The resulting solid was then transferred to a clean vial. To facilitate cocrystal growth, a saturated solution of the ground mixture was prepared in acetone (ACE) and filtered into a separate vial. The solution was left undisturbed to allow slow solvent evaporation, leading to the formation of the cocrystal.

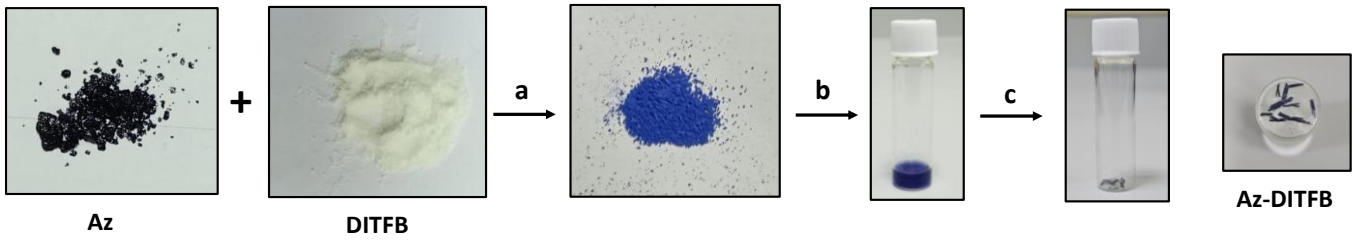

Scheme S2: (a) Mix Az and DITFB with a few drops of methanol, and grind the mixture using a mortar and pestle. Dry the resulting solid. (b) Dissolve the dried solid in methanol and filter the solution into a vial. (c) Allow the solvent to evaporate slowly over 3-4 days.

Section C: Tables

Table S1: Crystallographic data and refinement parameters for Az-TCNB cocrystal.

Parameters	Az-TCNB
Formula	$C_{20}H_{10}N_4$
Formula weight	306.32
Crystal system	Monoclinic
Space group, Z	*C 2/m*
a (Å)	9.3261(3)
b (Å)	12.5443(4)
c (Å)	6.6892(3)
α (deg)	90
β (deg)	107.9040(10)
γ (deg)	90
Volume, $Å^3$	744.67(5)
R factor	3.20
Temp (K)	293
$Density_{calc}$ (g/cm^3)	1.366
No. of reflections collected	11017
Independent reflections	969
$2\theta_{max}$ (deg)	56.9
R indices, wR2, [I>2sigma(I)]	0.0320, 0.0907
R indices, wR2 (all data)	0.0359, 0.0941
Goodness of fit	1.084
CCDC number	2530205

Table S2: Interaction energies and SAPT(0) energy components for selected dimers of cocrystals Az-TCNB and Az-DITFB determined by SAPT(0)/def2-SVP.

	Dimers	Electrostatic (kJ/mol)	Exchange (kJ/mol)	Induction (kJ/mol)	Dispersion (kJ/mol)	$E^{SAPT(0)}$ (kJ/mol)
Az-TCNB	DA1	-50.04	77.50	-15.86	-71.09	-59.49
	DA2	-1.21	7.75	-1.51	-7.87	-2.84
	DA3	-7.49	8.55	-1.58	-10.05	-10.57
Az-DITFB	DA4	-24.35	37.05	-10.77	-22.77	-20.83
	DA5	-13.93	25.75	-6.51	-18.46	-13.15
	DA6	-5.28	10.46	-1.18	-10.57	-6.57

Table S3: Mean position (POS), participation ratio (PR), charge transfer character (CT) of excited states Az-TCNB and Az-DITFB computed at LC-ωhPBE/def2-SVP level of theory.

	State	E (eV)	POS	PR	CT
Az-TCNB	S_1	2.199	1.974	1.054	0.051
	S_2	3.258	1.496	1.064	0.940
	S_3	3.833	1.972	1.058	0.054
	S_4	4.053	1.507	1.080	0.926
	S_5	4.513	1.502	1.056	0.947
Az-DITFB	S_1	2.443	1.006	1.013	0.012
	S_2	3.967	1.009	1.018	0.017
	S_3	4.768	1.989	1.023	0.019
	S_4	4.998	1.094	1.206	0.027
	S_5	5.038	1.855	1.328	0.096

Table S4: TD-DFT Vertical excitation energies of Az-TCNB and Az-DITFB computed at LC-ωhPBE/def2-SVP level of theory.

	State	E (eV)	State	E (eV)
Az-TCNB	S_1	2.199	T_1	0.301
	S_2	3.258	T_2	1.722
	S_3	3.833	T_3	2.291
	S_4	4.053	T_4	2.655
	S_5	4.513	T_5	3.119
	S_6	4.835	T_6	3.852
	S_7	4.906	T_7	3.951
Az-DITFB	S_1	2.443	T_1	0.497
	S_2	3.967	T_2	1.928
	S_3	4.768	T_3	2.848
	S_4	4.998	T_4	3.042
	S_5	5.038	T_5	3.894
	S_6	5.177	T_6	4.035
	S_7	5.227	T_7	4.261

Table S5: TD-DFT Vertical excitation energies of Az, TCNB and DITFB computed at LC-ωhPBE/def2-SVP level of theory.

	State	E (eV)	State	E (eV)
Az	S_1	2.291	T_1	1.579
	S_2	4.164	T_2	1.803
	S_3	5.477	T_3	3.014
	S_4	5.575	T_4	4.447
	S_5	6.489	T_5	4.954
	S_6	6.722	T_6	6.026
	S_7	6.879	T_7	6.113
TCNB	S_1	4.952	T_1	2.332
	S_2	5.267	T_2	4.022
	S_3	6.213	T_3	4.328
	S_4	6.592	T_4	4.737
	S_5	6.662	T_5	5.163
	S_6	6.684	T_6	5.460
	S_7	6.745	T_7	5.938
DITFB	S_1	4.748	T_1	3.179
	S_2	4.980	T_2	4.019
	S_3	5.174	T_3	4.163
	S_4	5.181	T_4	4.294
	S_5	5.396	T_5	4.299
	S_6	5.822	T_6	4.349
	S_7	5.870	T_7	4.808

Table S6: Gated emission life-time of Az-DITFB measured at 77 K and 298 K.

	77 K	298 K
λ_{Max}^{Demi} in nm	552	511
τ in μs	326.23	62.73

Table S7: Spin-orbit coupling values between the singlet and triplet states of Az-TCNB and Az-DITFB calculated at the CAM-B3LYP/def2-SVP level of theory.

Az-TCNB		Az-DITFB	
Transition	**cm^{-1}**	**Transition**	**cm^{-1}**
$\langle S_2 \vert H_{SOC} \vert T_1 \rangle$	0.6734	$\langle S_2 \vert H_{SOC} \vert T_1 \rangle$	0.5690
$\langle S_2 \vert H_{SOC} \vert T_2 \rangle$	0.0090	$\langle S_2 \vert H_{SOC} \vert T_2 \rangle$	2.0149
$\langle S_2 \vert H_{SOC} \vert T_3 \rangle$	1.1502	$\langle S_2 \vert H_{SOC} \vert T_3 \rangle$	0.0639
$\langle S_2 \vert H_{SOC} \vert T_4 \rangle$	0.0053	$\langle S_2 \vert H_{SOC} \vert T_4 \rangle$	0.2027
$\langle S_2 \vert H_{SOC} \vert T_5 \rangle$	0.0836	$\langle S_2 \vert H_{SOC} \vert T_5 \rangle$	0.1688
$\langle S_2 \vert H_{SOC} \vert T_6 \rangle$	0.0522	$\langle S_2 \vert H_{SOC} \vert T_6 \rangle$	2.1051
$\langle S_2 \vert H_{SOC} \vert T_7 \rangle$	0.0476	$\langle S_2 \vert H_{SOC} \vert T_7 \rangle$	0.6673
$\langle S_2 \vert H_{SOC} \vert T_8 \rangle$	0.4184	$\langle S_2 \vert H_{SOC} \vert T_8 \rangle$	0.2744
$\langle S_2 \vert H_{SOC} \vert T_9 \rangle$	0.0504	$\langle S_2 \vert H_{SOC} \vert T_9 \rangle$	0.0593
$\langle S_2 \vert H_{SOC} \vert T_{10} \rangle$	0.0483	$\langle S_2 \vert H_{SOC} \vert T_{10} \rangle$	2.1083

Table S8: Relative % intermolecular interactions obtained from Hirshfeld analysis of Az-TCNB and Az-DITFB cocrystal.

Interaction	Az-TCNB	Az-DITFB
%C•••C	13.8	1.5
%C•••H	6.6	7.4
%H•••H	21.9	7.2
%N•••H	53.2	Nil
%N•••C	2.3	Nil
%N•••N	2.2	Nil
%H•••F	Nil	30.1
%F•••I	Nil	12.2
%H•••I	Nil	12.1
%C•••F	Nil	11.8
%C•••I	Nil	11.8
%F•••F	Nil	5.3
%I•••I	Nil	0.7

Section D: Figures

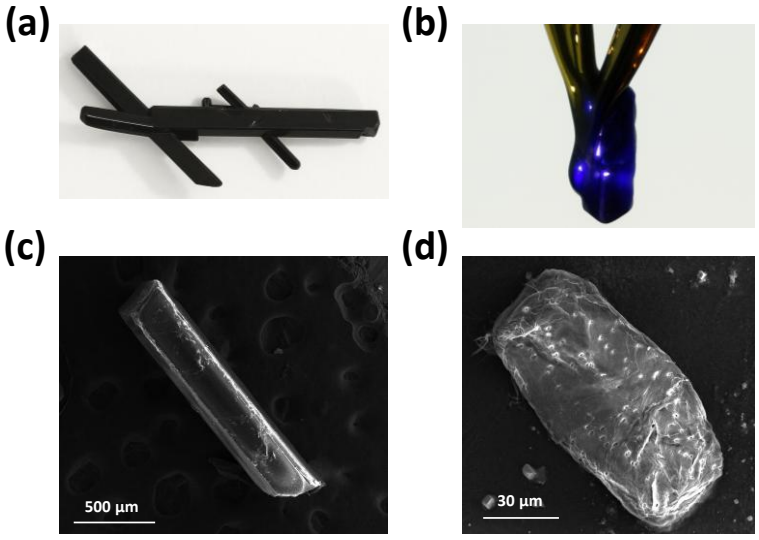

Fig. S1: Crystals of a) Az-TCNB and b) Az-DITFB. SEM image of c) Az-TCNB and d) Az-DITFB.

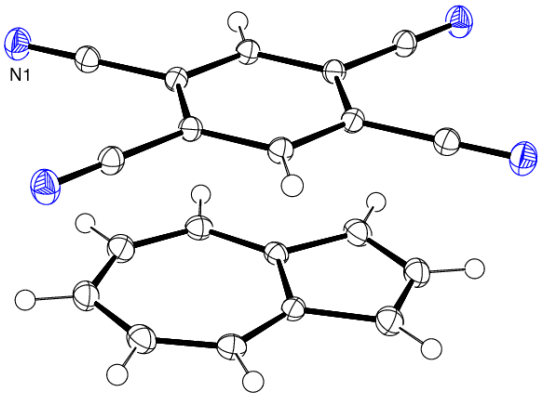

Fig. S2: ORTEP diagram of Az-TCNB.
In cocrystal Az-TCNB, the azulene molecule exhibits whole-molecule disorder across the crystallographic inversion center, with two mutually inverted orientations refined at equal occupancy (0.5), resulting in a 50:50 disorder of the azulene moiety.

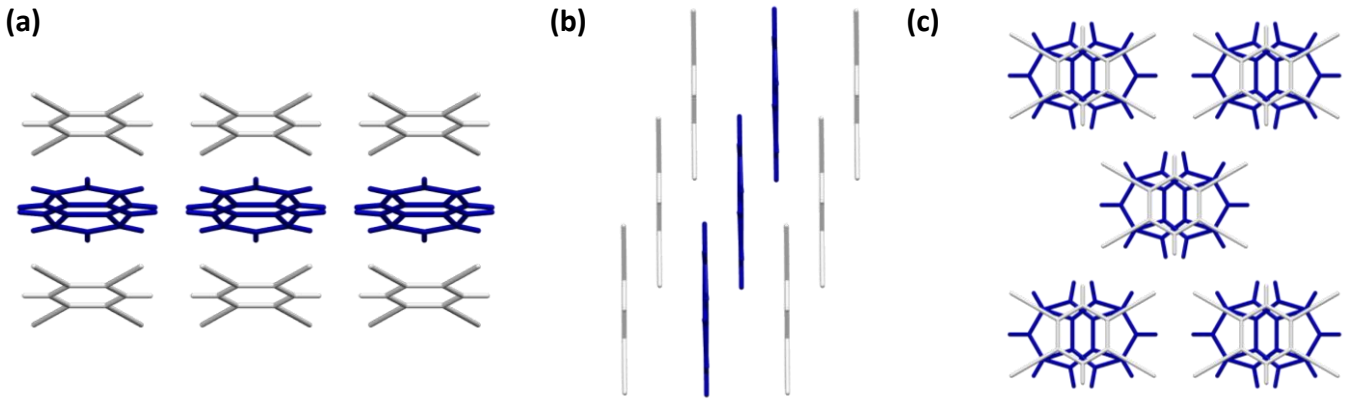

Fig. S3: Crystal packing of Az-TCNB viewed along (a) a, (b) b, and (c) c axis, respectively.

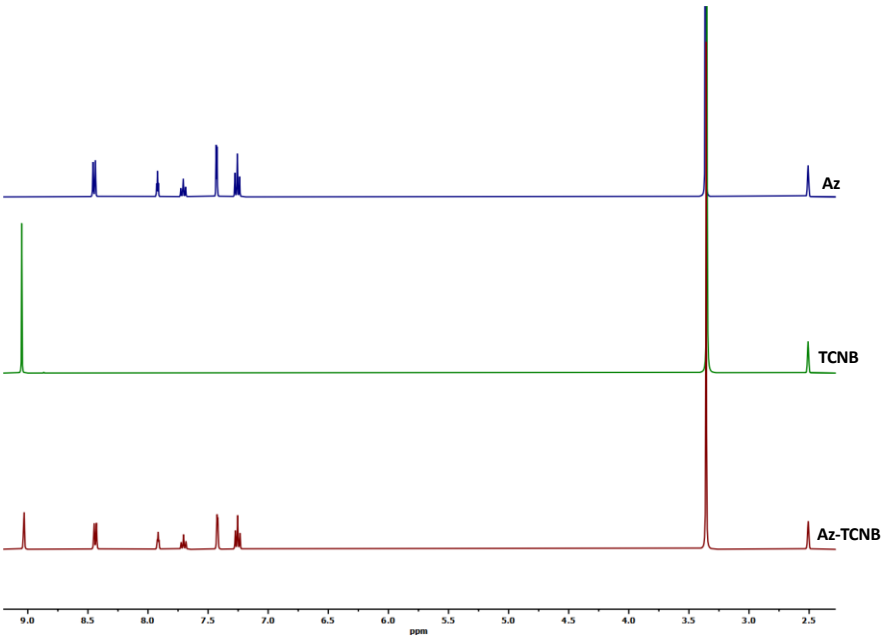

Fig. S4: ^{1}H NMR spectra of Az, TCNB and Az-TCNB cocrystal in DMSO-d_6.

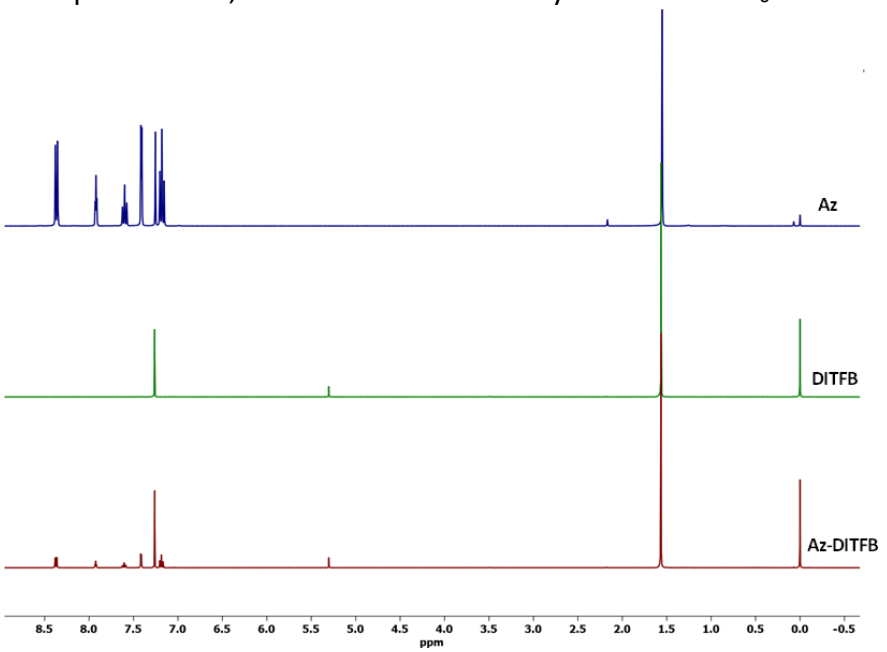

Fig. S5: ^{1}H NMR spectra of Az, DITFB and Az-DITFB cocrystal in $CDCl_3$.

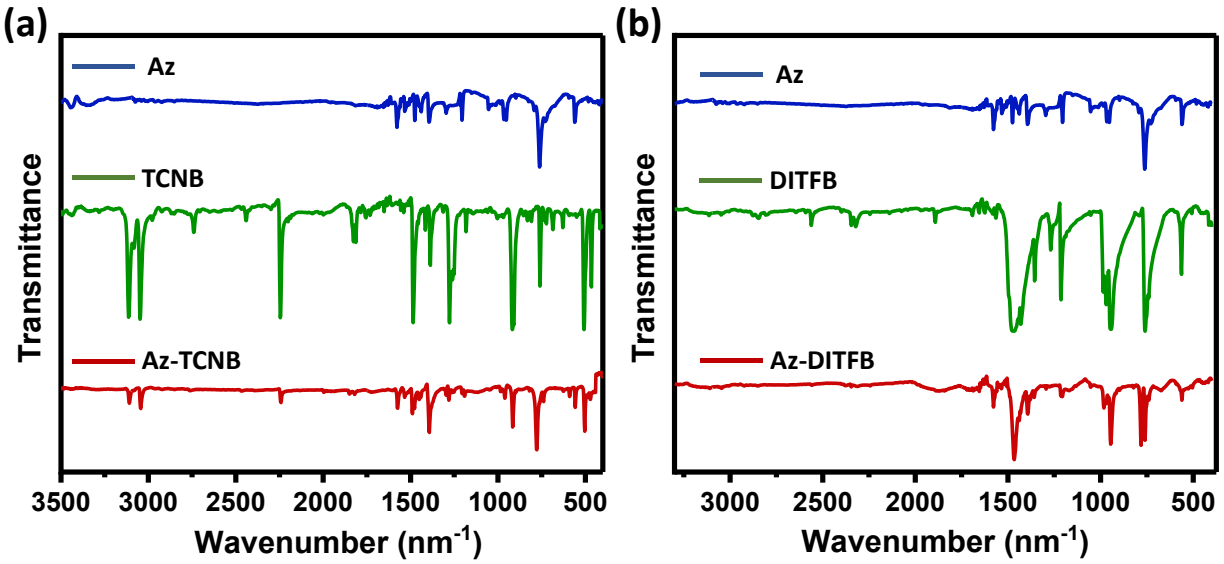

Fig. S6: Overlay of IR spectra of a) Az, TCNB, and Az- TCNB b) Az, DITFB, and Az- DITFB.

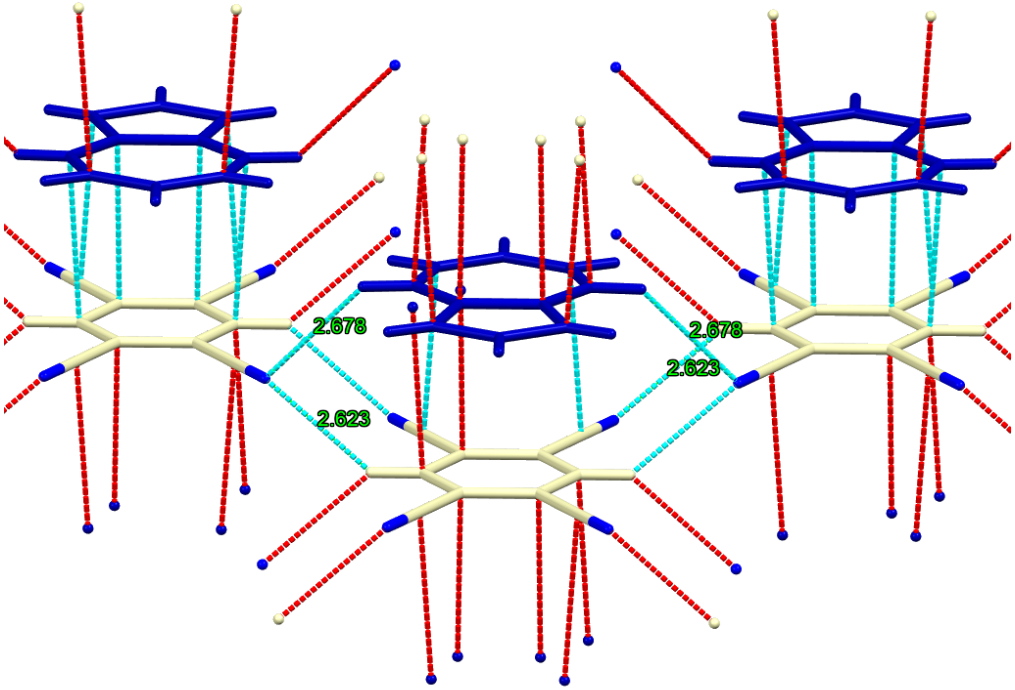

Fig. S7: Additional stabilizing interactions present in Az-TCNB cocrystal.

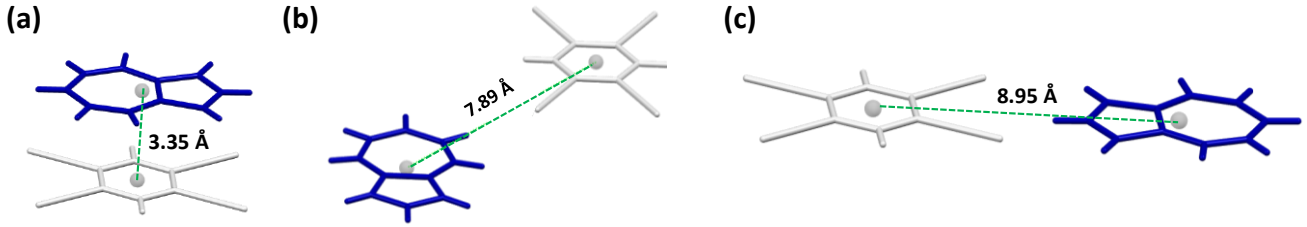

Fig. S8: Identified dimers a) DA1, b) DA2 and c) DA3 of Az-TCNB cocrystal with centroid-to-centroid distance in Å.

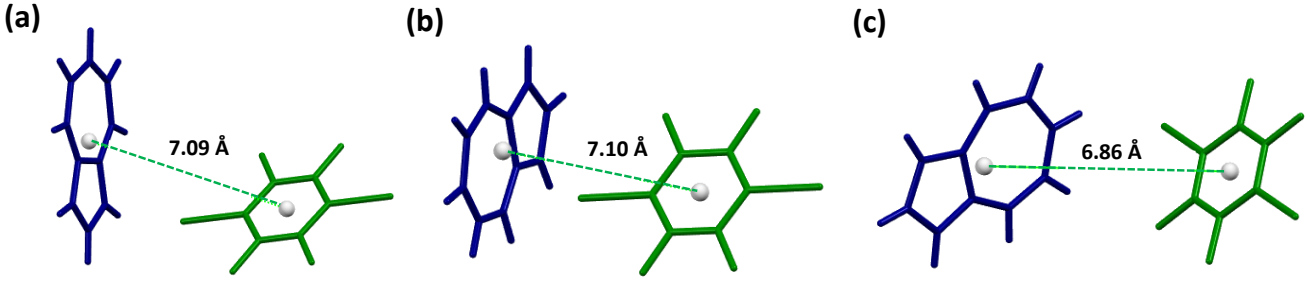

Fig. S9: Identified dimers a) DA4, b) DA5 and c) DA6 of Az-DITFB cocrystal with centroid-to-centroid distance in Å.[17]

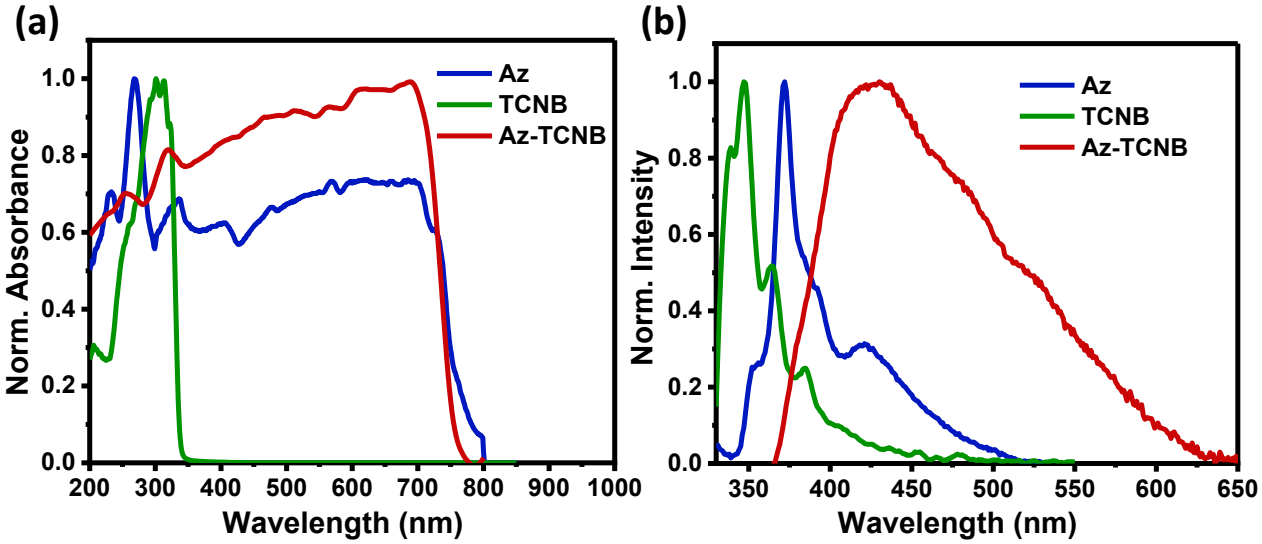

Fig. S10: (a) Normalized Kubelka-Munk transformed diffuse reflectance spectra and (b) steady-state emission spectra of Az (donor), TCNB (acceptor) and Az-TCNB (cocrystal).

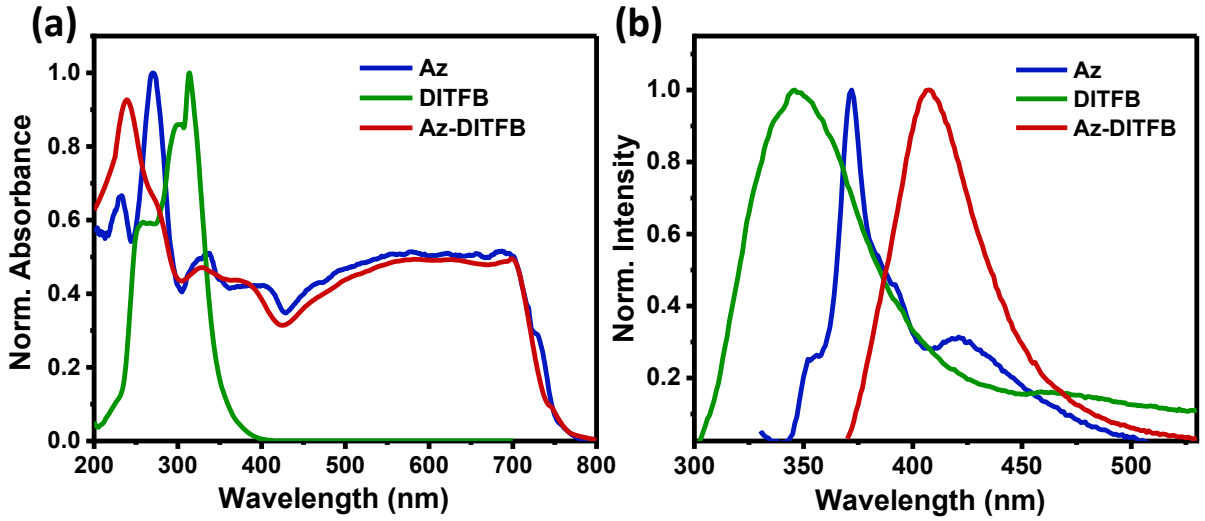

Fig. S11: (a) Normalized Kubelka-Munk transformed diffuse reflectance spectra and (b) steady-state emission spectra of Az (donor), DITFB (acceptor) and Az-DITFB (cocrystal).

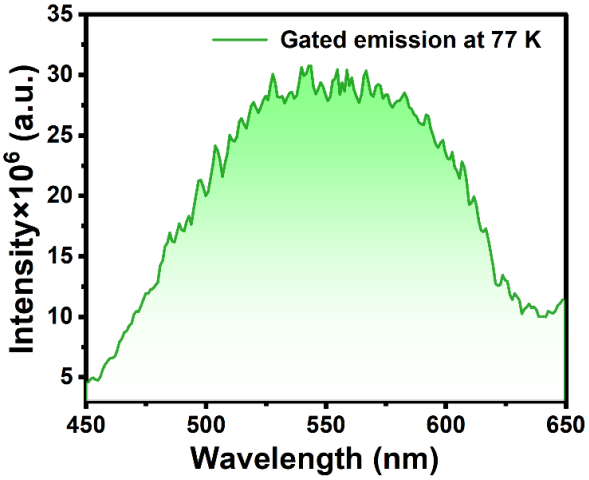

Fig. S12: Gated emission spectrum of Az-DITFB at 77 K (excited at 360 nm). The intensity of the gated

emission is enhanced sevenfold at 77 K compared to 298 K.

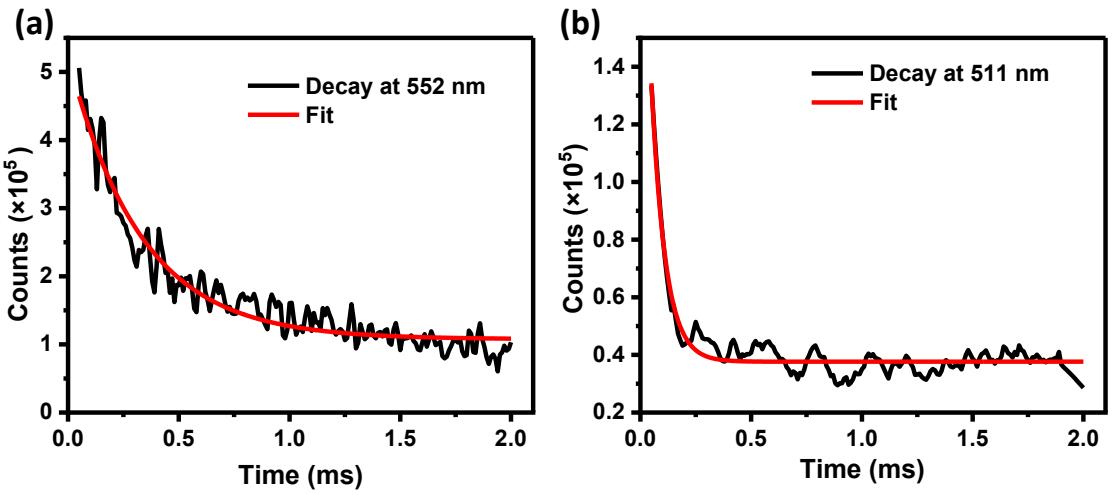

Fig. S13: Decay profiles of gated emission of Az-DITFB (collected at its emission maximum) at (a) 77 K and (b) 298 K (delay time = 50 μs).

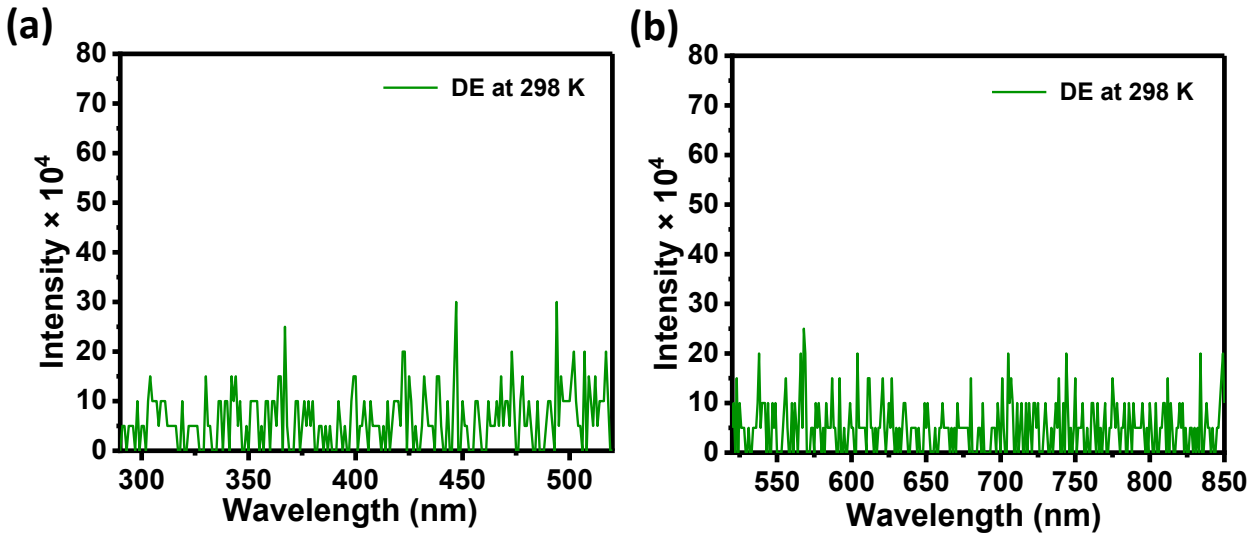

Fig. S14: Gated emission spectrum of Az-TCNB (a) excited at 270 nm and (b) excited at 500 nm.

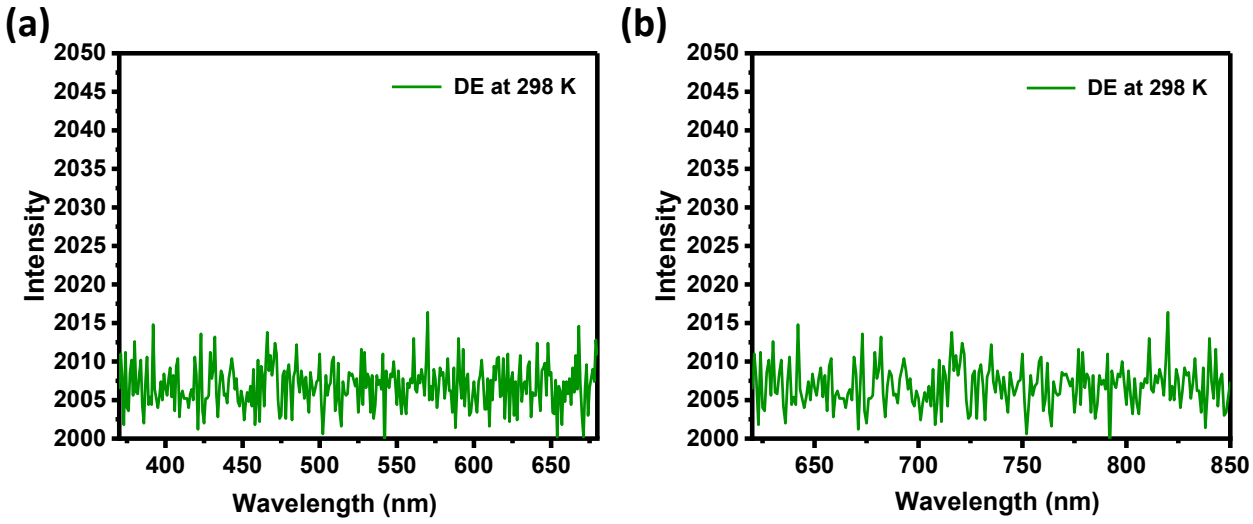

Fig. S15: Gated emission spectrum of Az (a) excited at 350 nm and (b) excited at 600 nm.

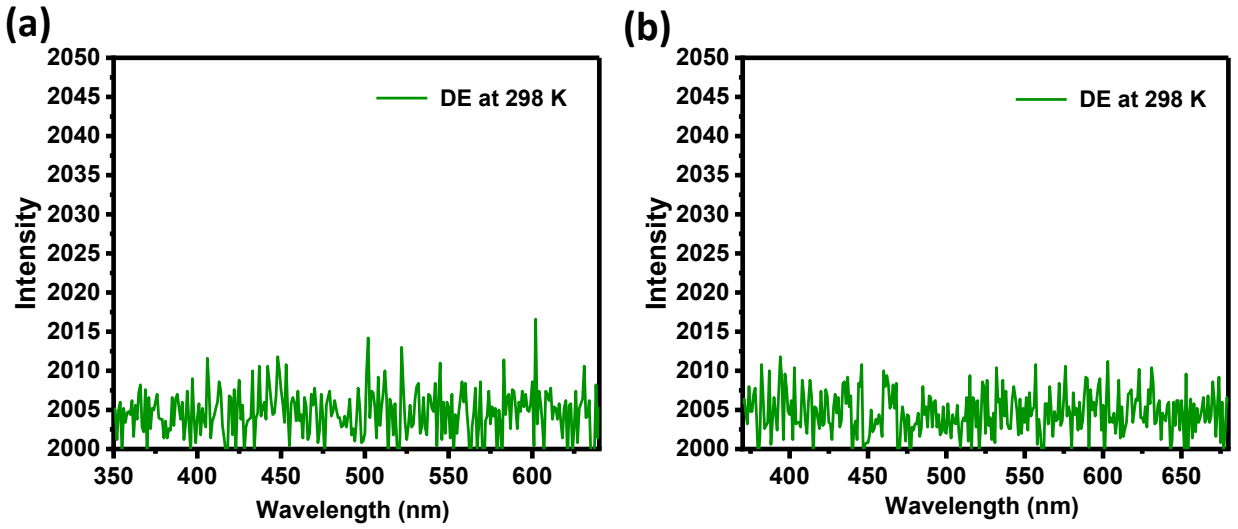

Fig. S16: Gated emission spectra of (a) TCNB excited at 330 nm and (b) DITFB excited at 350 nm.

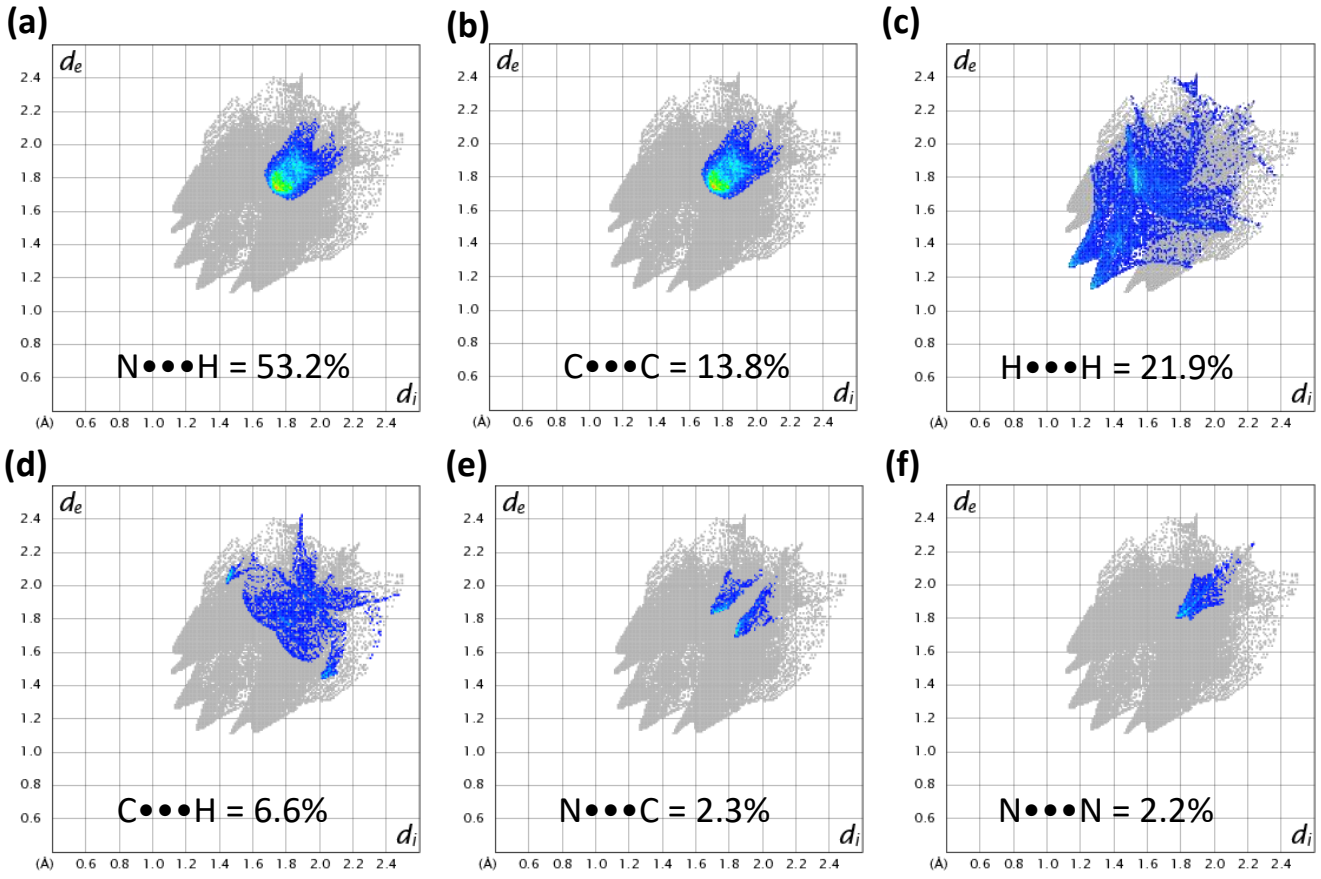

Fig. S17: Hirshfeld 2D fingerprint plots a) N•••H b) C•••C, c) H•••H, d) C•••H, e) N•••C and f) N•••N interactions of Az-TCNB cocrystal.

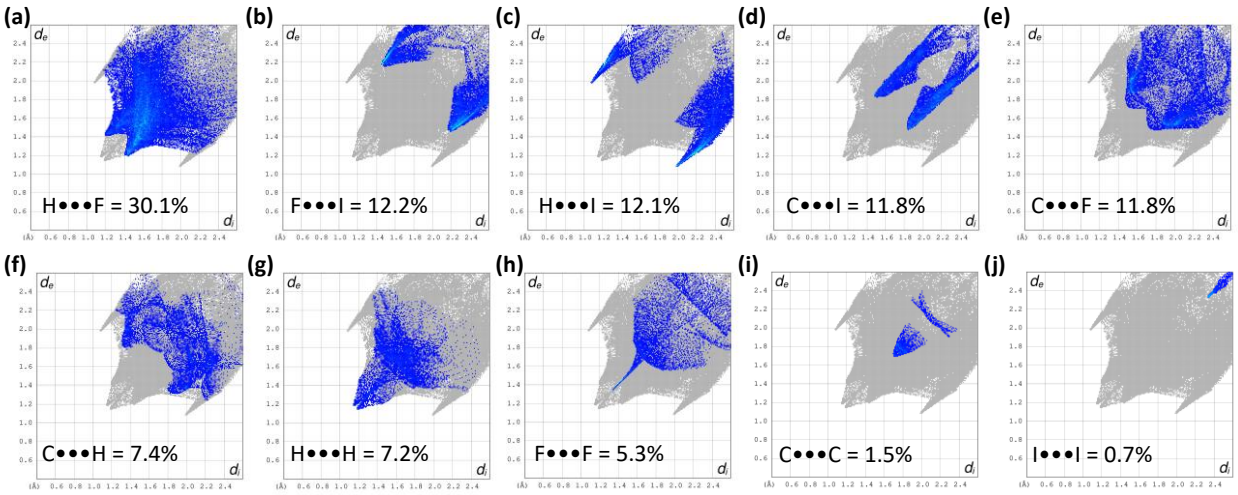

Fig. S18: Hirshfeld 2D fingerprint plots a) H•••F b) F•••I, c) H•••I, d) C•••I, e) C•••F f) C•••H, g) H•••H, h) F•••F, i) C•••C and j) I•••I interactions of Az-DITFB cocrystal.

Coordinates

(a) Az-TCNB

0 1

C	2.32710000	1.42400000	0.76480000
C	1.14240000	0.70410000	0.37150000
C	0.00000000	1.40670000	0.00000000
H	0.00000000	2.33680000	0.00000000
N	3.26990000	1.99450000	1.08280000
C	-2.32710000	1.42400000	-0.76480000
C	-1.14240000	0.70410000	-0.37150000
N	-3.26990000	1.99450000	-1.08280000
C	-2.32710000	-1.42400000	-0.76480000
C	-1.14240000	-0.70410000	-0.37150000
C	0.00000000	-1.40670000	0.00000000
H	0.00000000	-2.33680000	0.00000000
N	-3.26990000	-1.99450000	-1.08280000
C	2.32710000	-1.42400000	0.76480000
C	1.14240000	-0.70410000	0.37150000
N	3.26990000	-1.99450000	1.08280000
C	0.77310000	1.20380000	3.78870000
C	1.43170000	0.00000000	4.00970000
H	2.31340000	0.00000000	4.30560000
C	-1.60380000	1.59610000	3.01710000
H	-1.45140000	2.51040000	3.09410000
C	-0.56390000	0.74830000	3.36210000
H	1.21000000	2.00710000	3.95920000
C	-2.82950000	1.20380000	2.57650000
C	-3.48810000	0.00000000	2.35550000
H	-4.36990000	0.00000000	2.05970000
H	-3.26650000	2.00710000	2.40610000
C	-2.82950000	-1.20380000	2.57650000
H	-3.26650000	-2.00710000	2.40610000
C	0.77310000	-1.20380000	3.78870000
C	-1.60380000	-1.59610000	3.01710000
H	-1.45140000	-2.51040000	3.09410000
C	-0.56390000	-0.74830000	3.36210000
H	1.21000000	-2.00710000	3.95920000

(b) Az-DITFB

0 1

C	7.39300000	0.74360000	2.59830000
H	8.09360000	0.68890000	1.95940000
C	6.25040000	-0.07090000	2.63210000
H	6.05230000	-0.75940000	2.00920000
C	5.44550000	0.28520000	3.72310000
H	4.62340000	-0.12600000	3.96360000
C	6.05620000	1.34590000	4.39910000
C	5.57580000	1.98120000	5.52390000
H	4.75700000	1.64330000	5.86810000
C	6.12000000	3.03420000	6.21550000
H	5.60030000	3.35030000	6.94560000
C	7.32650000	3.71200000	6.00660000
H	7.52630000	4.39400000	6.63750000
C	8.26750000	3.53050000	5.01160000
H	9.01770000	4.11170000	5.04730000
C	8.27050000	2.61210000	3.96020000
H	9.01840000	2.65760000	3.37630000
C	7.32690000	1.64520000	3.65820000
C	10.38220000	-4.81070000	7.95280000
C	9.21870000	-5.29120000	7.36290000
C	8.49330000	-4.52220000	6.48080000
F	7.37940000	-5.04830000	5.94300000
F	8.80130000	-6.54320000	7.62200000
I	11.48760000	-5.98070000	9.27480000
C	8.87610000	-3.23280000	6.16050000
C	10.03960000	-2.75230000	6.75040000
C	10.76490000	-3.52130000	7.63250000
F	11.87880000	-2.99510000	8.17030000
F	10.45690000	-1.50030000	6.49130000
I	7.77060000	-2.06270000	4.83850000

References

1. Y. Zhang, J. Sun, G. Zhuang, M. Ouyang, Z. Yu, F. Cao, G. Pan, P. Tang, C. Zhang and Y. Ma, *J. Mater. Chem. C*, 2013, **2**, 195–200.
2. J. Gierschner, S. Varghese and S. Y. Park, *Adv. Opt. Mater.*, 2016, **4**, 348–364.
3. G. M. Sheldrick, *Acta Crystallogr. A*, 2008, **64**, 112–122.
4. A. L. Spek, *J. Appl. Crystallogr.*, 2003, **36**, 7–13.
5. L. J. Farrugia, *J. Appl. Crystallogr.*, 1999, **32**, 837–838.
6. I. J. Bruno, J. C. Cole, P. R. Edgington, M. Kessler, C. F. Macrae, P. McCabe, J. Pearson and R. Taylor, *Acta Crystallogr. B*, 2002, **58**, 389–397.
7. C. F. Macrae, I. J. Bruno, J. A. Chisholm, P. R. Edgington, P. McCabe, E. Pidcock, L. Rodriguez-Monge, R. Taylor, J. van de Streek and P. A. Wood, *J. Appl. Crystallogr.*, 2008, **41**, 466–470.
8. Gaussian 16, Revision B.01, Frisch, M.J., Trucks, G.W., Schlegel, H.B., Scuseria, G.E., Robb, M.A., Cheeseman, J.R.; Scalmani, G.; Barone, V.; Petersson, G.A.; Nakatsuji, H.; Li, X.; Caricato, M.; Marenich, A.V.; Bloino, J., Janesko, B.G., Gomperts, R., Mennucci, B., Hratchian, H.P., Ortiz, J.V., Izmaylov, A.F., Sonnenberg, J.L., Williams-Young, D., Ding, F., Lipparini, F., Egidi, F., Goings, J., Peng, B., Petrone, A., Henderson, T., Ranasinghe, D., Zakrzewski, V.G., Gao, J., Rega, N., Zheng, G., Liang, W., Hada, M., Ehara, M., Toyota, K., Fukuda, R., Hasegawa, J., Ishida, M., Nakajima, T., Honda, Y., Kitao, O., Nakai, H., Vreven, T., Throssell, K., Montgomery Jr., J.A., Peralta, J.E., Ogliaro, F., Bearpark, M.J., Heyd, J.J., Brothers, E.N., Kudin, K.N., Staroverov, V.N., Keith, T.A., Kobayashi, R., Normand, J., Raghavachari, K., Rendell, A.P., Burant, J.C., Iyengar, S.S., Tomasi, J., Cossi, M., Millam, J.M., Klene, M., Adamo, C., Cammi, R., Ochterski, J.W., Martin, R.L., Morokuma, K., Farkas, O., Foresman, J.B., Fox, D.J. Gaussian, Inc., Wallingford CT (2016) GaussView 5.0. Wallingford, E.U.A.
9. R. M. Parrish, L. A. Burns, D. G. A. Smith, A. C. Simmonett, A. E. DePrince, III, E. G. Hohenstein, U. Bozkaya, A. Y. Sokolov, R. Di Remigio, R. M. Richard, J.F. Gonthier, A. M. James, H. R. McAlexander, A. Kumar, M. Saitow, X. Wang, B. P. Pritchard, P.Verma, H. F. Schaefer, III, K. Patkowski, R. A. King, E. F.Valeev, F. A. Evangelista, J. M. Turney, T. D.

Crawford and C. D. Sherrill, J. Chem. Theory Comput., 2017, 13, 3185-3197.
10. F. Plasser and H. Lischka, *J. Chem. Theory Comput.*, 2012, **8**, 2777–2789.
11. F. Plasser, J. Chem. Phys., 2020, 152, 084108.
12. C. K. Robinson, M. Weinrich and S. E. Lewis, *Chem. Educ. Res. Pract.*, 2025, **26**, 647–659.
13. X. Gao, S. Bai, D. Fazzi, T. Niehaus, M. Barbatti and W. Thiel, *J. Chem. Theory Comput.*, 2017, **13**, 515–524.
14. J. Contreras-García, E. R. Johnson, S. Keinan, R. Chaudret, J.-P. Piquemal, D. N. Beratan and W. Yang, *J. Chem. Theory Comput.*, 2011, **7**, 625–632.
15. S. K. Rajagopal, A. M. Philip, K. Nagarajan and M. Hariharan, *Chem. Commun.*, 2014, **50**, 8644–8647.
16. M. A. Spackman and D. Jayatilaka, *CrystEngComm*, 2009, **11**, 19–32.
17. J. Vainauskas, F. Topić, O. S. Bushuyev, C. J. Barrett and T. Friščić, *Chem. Commun.*, 2020, **56**, 15145–15148.